北海道大学　大学院工学　ロゼロナバロ　ナタリーカロリーナ

Nano Glass-Ceramic Lithium-Ion Conductive Buffer Layers for High Li-Ion Transport at Electrode/Electrolyte Interface for All-Solid-State Batteries

Nataly Carolina Rosero-Navarro
Division of Applied Chemistry, Faculty of Engineering, Hokkaido University, Japan
Current Affiliation. Institute of Ceramic and Glass ICV-CSIC, Spain

Nano glass-ceramic lithium-ion conductive buffer layers with controlled composition and crystallization were prepared to generate stable Li-ion transport at the Li|solid electrolyte interface under high current densities. In particular, Li_2O-B_2O_3 glass was used as a sintering additive and interfacial buffer layer to modify the microstructure of $Li_{6.5}La_3Zr_{1.5}Ta_{0.5}O_{12}$ (LLZT) and enhance the Li|LLZT interfacial resistance. The effect of the Li_2O-B_2O_3 addition as sol on the sintering behaviour of LLZT was investigated and compared with those using Li_2O-B_2O_3 as powder. The ionic conductivity of the LLZT sintered with addition of Li_2O-B_2O_3 sol and Li_2O-B_2O_3 powder achieves 8×10^{-4} S cm^{-1} (94%) and 6.3×10^{-5} S cm^{-1} (78%) at room temperature, respectively. Moreover, Li|LLZT interfacial resistance became lower than those without the use of Li_3BO_3, achieving a critical current density of 10 mA cm^{-2}. The results suggest that the interfacial inorganic layer can favour not only the sintering of solid oxide-type electrolytes but also the interfacial electrode/electrolyte resistances.

1. Introduction

All-solid-state batteries are one of the most promising candidates for energy storage systems with high energy density. Nowadays, several solid electrolytes with exceptional high ionic conductivities and wide electrochemical windows have been obtained, making them not only compatible with high-potential electrodes but also a safe alternative for energy storage. Although the advantages of the solid electrolytes, the realization of all-solid-state batteries still remains elusive mainly due to high electrode/electrolyte interface resistance. All-solid-state batteries based on oxide-type solid electrolytes ($Li_{6.5}La_3Zr_{1.5}Ta_{0.5}O_{12}$, LLZT) are of particular interest because of chemical compatibility with lithium metal as anode. In this regard, the main challenge is to reduce the interfacial Li/solid electrolyte resistance and prevent the dendrite formation at high current densities.

Li alloys [1,2] are one of the most used strategies to reduce the interfacial resistance between LLZ ($Li_7La_3Zr_2O_{12}$,) solid electrolyte and lithium metal (Li|LLZ interface). Our group[3] have proposed the use of an amorphous Li_2O-SiO_2 buffer coating. These strategies significantly reduce the Li|LLZ interfacial resistance. However, the current limit density, at which the cell is shorted by lithium dendrite formation, is still low and far from the current density required for the fast-charge goal (10 mA cm^{-2})[4]. Ideally, new alternatives to handle free-dendrites Li|solid electrolyte interface at high current density should have adequate

Li-ion conductivity allowing for the stable distribution of the high current densities and maintaining the integrity of the solid-solid contacts. In this sense, the lithium alloys seem impractical as the large volume changes[5] (e.g. 100–400% for Li–Si and Li–Al alloys) could certainly threaten the integrity of solid-solid contacts.

In this work, the synthesis of low-temperature oxide-type solid electrolytes by using sintering glassy Li_2O-B_2O_3 additives is presented. The use of amorphous Li_2O-B_2O_3 interfacial material is used to overcome the rigid nature of ceramic-oxide solid electrolytes. Inorganic Li_2O-B_2O_3 interfacial material is a promising alternative to prepare all-solid-state batteries producing enough physical contacts between solid electrolyte and electrodes. This report includes results already partially published. [6,7]

2. Experimental Section

Synthesis of materials. The synthesis of Ta-doped LLZ by the sol-gel process was carried out following a reported procedure[8]. First, $LiNO_3$ (99%, Kanto chemicals) and $La(NO_3)_3 \cdot 6H_2O$ (99.9%, Kanto chemicals) were dissolved in ethanol. Second, $Ta(OC_2H_5)_5$ (99.9%, High-purity chemicals), $Zr(OC_4H_9)_4$ (85% in butanol, Wako pure chemicals) and ethyl acetoacetate (EAcAc, 99%, Kanto chemicals) were dissolved in ethanol under argon atmosphere and stirred for 1 hour. Then, both solutions were mixed, and the resulted transparent solution was stirred at room temperature for 1 to 2 hours to obtain a sol. The obtained sol was dried under vacuum between 80 and 130℃ to obtain a dried gel that was later pulverized and heat-treated at 700℃ in an alumina crucible for 5 hours (1℃ min-1). Finally, 2 g of this powder and 4 mL of toluene were placed in a ZrO2 pot and grounded at 300 RPM for 6 hours. Then, toluene was evaporated under vacuum at 100℃ to obtain final LLZT calcined powder. The molar ratio of Li:La:Zr:Ta:EAcAc was 7.15:3:1.3:0.5:1.5 and lithium was added in 10% excess to compensate for the loss of Li during sintering. The Li_2O-B_2O_3 sol was synthesized by the sol-gel process using trimethoxyborane (TMB, Shin-Etsu Chemicals) and lithium ethoxide (High-purity chemicals) in a molar ratio 3:1 and total concentration of 40 gL-1. TMB was dissolved in ethanol and stabilized by addition of EAcAc under argon atmosphere. Then, 0.1M HNO_3 was added dropwise (molar ratio TMB:HNO_3 of 1:0.5), and the mixture was stirred for 1 hour. In parallel, lithium ethoxide was dissolved in ethanol. Then, both solutions, TMB and lithium ethoxide, were mixed and stirred for 1 hour to obtain a precursor LBO solution. The LBO powder was synthesized by the solid-state process following a reported procedure[8,9]. Briefly, the Li_2O (Wako pure chemicals) and B_2O_3 (Wako pure chemicals) in a molar ratio 3:1 were ball milled under an argon atmosphere for 40 hours under 370 RPM. Then, the milled powder was heat-treated at 210℃ for 10 hours and finally to 600℃ for 5 hours to obtain Li_3BO_3 powder. The Al_2O_3 sol and powder were obtained by commercial source with particle size～50 nm and～1 μm, respectively. Both materials were used without any further purification or pretreatment.

Sintering of LLZT pellets. LBO and Al_2O_3, sols and/or powders, were added to the LLZT calcined powder and mixed in a mortar using toluene. Toluene was completely removed at 80℃ for approximately 2 hours. The calcinated LLZT powder containing sintering additives

were formed into pellets (Ø=10mm) at 100MPa (5min) using a uniaxial press and then, were sintered at 1000℃ (10h) using a heating rate of 1℃ /min and intermedium step at 700℃ (5h). The pellets were sintered under ambient atmosphere using alumina crucibles. The pellets were thoroughly buried in identical powder to mitigate losses of lithium and prevent any contamination with crucibles.

Physicochemical Characterization. Crystal phase was determined by X-ray diffraction (XRD) using a RINT 2000 Ultima RIGAKU diffractometer. Powder samples were scanned between 10º and 60º at a rate of 2º/min using Cu-Kα radiation. Morphology of the cross-section pellets were observed by scanning electron microscopy (SEM), performed on a MultiFlex600 and JIB-4600F Multibeam SEM-FIB Scanning Electron Microscopes. The relative density was calculated with a geometrical dimension of the pellets and theoretical density of LLZT (5.11g cm-3).

Electrochemical characterization. HS Flat Cell HS-3ETK (Hohsen Corporation) was used to perform the electrochemical measurements. The conductivity of the composite solid electrolyte pellets was evaluated by the electrochemical impedance spectroscopy (EIS), under Ar atmosphere. The samples were Au-coated and sandwiched between two stainless-steel (SS, blocking electrodes) disks used as current collectors. Symmetric cells were constructed with lithium metal heated at 175℃ . EIS measurements were conducted using an impedance analyzer (SI 1260, Solartron) in the frequency range of 1-3MHz to 100Hz at the amplitude of 80-100mV. The impedance spectra were analyzed with ZView (Scribner Associates) to assess the ohmic total resistance (Rt), which was normalized to the pellet geometry (t: thickness and A: golden surface area) to calculate the conductivity through the usual formula $\sigma = t/Rt.A$.

3. Results and Discussion

The following cases were evaluated: (i) LBO and Al_2O_3 in the powder states, (ii) LBO in the sol state and Al_2O_3 in the powder state, and (iii) LBO and Al_2O_3 in the sol states (LLZT-PP, LLZT-SP, and LLZT-SS, denoting the state of each additive (powder or sol), respectively). XRD patterns of LLZT-PP, LLZT-SP, and LLZT-SS sintered at 1000℃ confirmed the formation of expected cubic phase with the $Ia\bar{3}d$ space group (ICSD #183607). LLZT-PP and LLZT-SP exhibited other peaks attributed to the tetragonal phase with the $I4_1/acd$ space group (ICSD #238686), $LaAlO_3$, and unidentified phases. The presence of the tetragonal phase is associated with the insufficient stabilization of the cubic phase, which suggests a nonuniform distribution of the sintering additives or insufficient amount of them, which could be the main reason for the promotion of secondary reactions during sintering. Nonetheless, the addition of solution-derived sintering additives leads to a single-phase cubic garnet structure with a lattice parameter in good agreement with that of LLZT (12.94Å)[8,9]. This confirms that the liquid phase of sintering additives formed during the sintering remains almost unreactive with LLZT grains and is present in the sintered ceramic body as an amorphous phase.

Figure1 shows cross-sectional SEM images of the LLZT pellets without and with sintering

additives, including the relative densities. The relative densities of LLZT, LLZT-PP, LLZT-SP, and LLZT-SS were 50 %, 78 %, 94 %, and 88 %, respectively. LLZT sintered in the absence of sintering additives exhibited a porous microstructure with single particles with a size of approximately 1 μm, indicating an insufficient densification. In contrast, the sintering additives positively contributed to the LLZT densification, where larger grains (above 20 μm) were observed as a clear signal of the grain growth and enhanced sintering. Notably, the relative densities of LLZT-PP and LLZT-SP were over- and under-estimated because these samples contained secondary phases as verified by XRD.

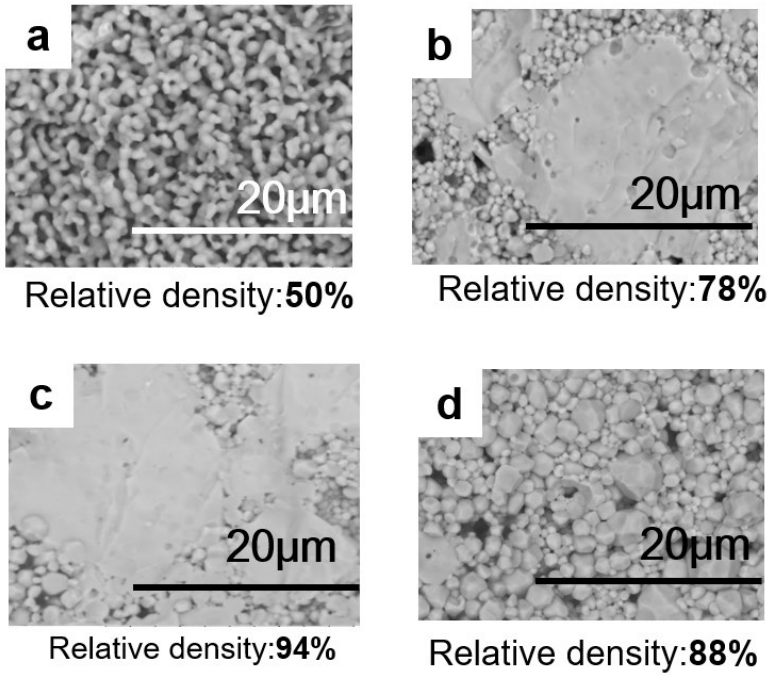

Figure 1. SEM image of cross section (a) LLZT without sintering additive, (b) LLZT-SS, (c) LLZT-SP, (d) LLZT-SS

Figure 2 (top) how Nyquist plots of the electrochemical impedance of the of *LLZT-PP, LLZT-SP and LLZT-SS* pellets measured at 25℃ . The semicircles at high frequencies (>10 kHz) are associated to the resistance of the LLZT composite electrolyte involving grains and grain boundaries. The tail at low frequencies is attributed the stainless-steel blocking electrodes. The total ionic conductivity (grain + grain boundary) calculated by the fitting of impedance profiles to the equivalent circuits was 0.063, 0.16, and 0.8 mS cm^{-1} for LLZT-PP, LLZT-SP, and LLZT-SS, respectively. Figure 2 (bottom) shows an Arrhenius plot of the LLZT

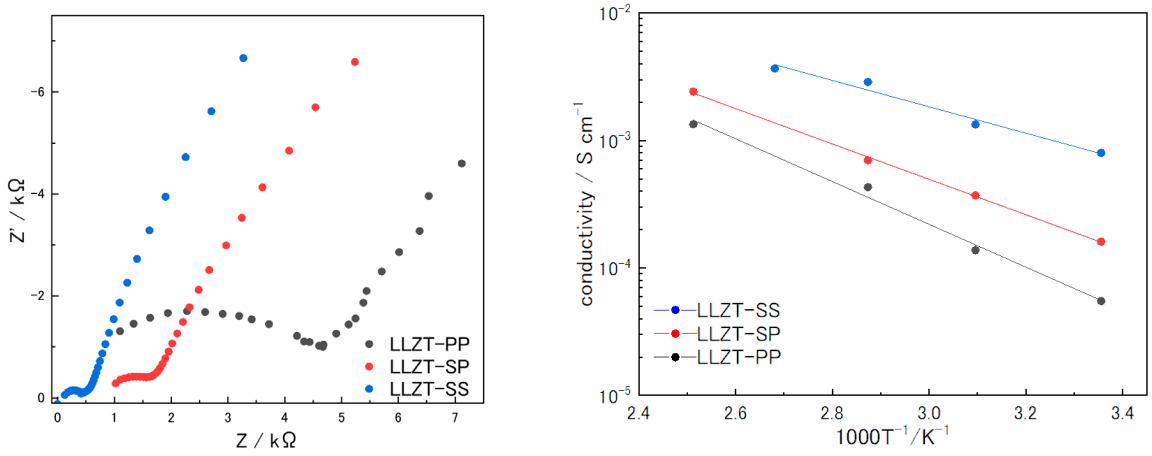

Figure 2. (top) Impedance profiles of LLZT-PP, LLZT-SP and LLZT-SS cells using blocking Au electrode at 25℃ . (bottom) Arrhenius plot.

pellets obtained by the total ionic conductivity in the temperature range of 25–125℃. The activation energy was 14, 12, and 9kJ mol^{-1} for LLZT-PP, LLZT-SP, and LLZT-SS, respectively. The lowest activation energy obtained when LLZT is sintered with LBO and Al_2O_3 sols is attributed to the low resistance of the grain boundaries. In other words, the ion mobility through the grain boundaries, formed by a more uniform distribution of LBO presumably located at the grain boundaries, is facilitated by the good contact between the LLZT grains and LBO. LBO in the solid electrolyte microstructure distributes the current homogeneously and prevents dendrite nucleation and propagation, suppressing lithium dendrites up to 10mA cm^{-2} (unpublished).

4. Conclusions

The effects of Li_2O–B_2O_3 and Al_2O_3 solution-derived sintering additives on the sinterability of LLZT solid electrolyte were studied and compared to their powder-state counterparts. The use of solution-derived sintering additives leads to a single-phase cubic garnet structure and enhanced densification. The use of in Li_2O–B_2O_3 and Al_2O_3 sintering of LLZT ceramic solid electrolyte achieves a high ionic conductivity of 0.8mS cm^{-1} at 25º with low activation energy (9kJ mol^{-1}) and almost negligible contribution of the grain boundary resistance (10%). The designed microstructure of the solid electrolytes plays a critical role in governing the electrochemical properties, particularly the CCD.

5. Acknowledgments

We would like to express our sincere gratitude to the grant organization of Nippon Sheet Glass Foundation for Materials Science and Engineering of Japan in 2021 for their kind support for the research activities of the current project.

References

[1] X. Han et al. Nature Materials 16, 572, 2016.
[2] K. Karthik, et al. Materials Today Energy 16, 100389, 2020.
[3] N.C. Rosero-Navarro et al. ACS Applied Energy Materials 3, 6, 5533–5541, 2020.
[4] P. Albertus et al. Nature Energy 3, 16–21, 2018.
[5] D Rehnlund et al. Energy Environ. Sci. 10, 1350– 1357, 2017.
[6] N.C. Rosero-Navarro et al. Journal of the European Ceramic Society 41, 6767–6771, 2021.
[7] N.C. Rosero-Navarro. Journal of Sol-Gel Science and Technology 103 (2), 680-689, 2022.
[8] N.C. Rosero-Navarro et al. Journal of Electronic Materials, 46, 497-501, 2017.
[9] N.C. Rosero-Navarro et al. Solid State Ionics, 285, 6-12. 2016.